



Mechanical strength of microspheres produced by drying of acoustically levitated suspension droplets



M. Kreimer^a, I. Aigner^a, S. Sacher^a, M. Krumme^b, T. Mannschott^b, P. van der Wel^c, A. Kaptein^c, H. Schroettner^{d,e}, G. Brenn^f, J.G. Khinast^{a,g,*}

^a Research Center Pharmaceutical Engineering (RCPE) GmbH, 8010 Graz, Austria

^b Novartis Pharma AG, Novartis Campus, 4056 Basel, Switzerland

^c Hosokawa Micron B.V., Gildenstraat 26, 7005 BL Doetinchem, Netherlands

^d Graz University of Technology, Institute for Electron Microscopy and Nanoanalysis, 8010 Graz, Austria

^e Austrian Centre for Electron Microscopy and Nanoanalysis (FELMI-ZFE), 8010 Graz, Austria

^f Graz University of Technology, Institute of Fluid Mechanics and Heat Transfer, 8010 Graz, Austria

^g Graz University of Technology, Institute for Process and Particle Engineering, 8010 Graz, Austria

ARTICLE INFO

Article history:

Received 3 July 2017

Received in revised form 14 September 2017

Accepted 3 November 2017

Available online 6 November 2017

Keywords:

Acoustic levitation

Spray drying

Suspensions

Microspheres

Morphology

Mechanical properties

ABSTRACT

Spray drying is widely used in pharmaceutical manufacturing to produce microspheres from solutions or suspensions. The mechanical properties of the microspheres are reflected by the morphology formed in the drying process. In suspension drying, solids dissolved in the carrier liquid may form bridges between the suspended primary particles, producing a microsphere structure which is resistant against mechanical loads. Experiments with individual, acoustically levitated droplets were performed to simulate the drying of suspension droplets in a spray drying process. The suspensions studied consisted of a binary liquid mixture as the carrier liquid, and primary particles of suspended lactose material which is partially soluble in the liquid. The solubility of lactose was varied by the composition of the liquid mixture. The experiments revealed longer first and second drying stages for higher lactose solubility. Electron micrographs revealed the morphology of individual microspheres produced by drying in the levitator. Microspheres with only primary particles and no visible crust were obtained for low lactose solubility, whereas higher contents of dissolved lactose resulted in a more densely packed microsphere with crust formation. To quantify the hardness of individual microspheres, the maximum breaking force upon mechanical loading was measured for a range of varying suspension compositions. These measurements confirmed that densely packed structures with a thick crust reveal high mechanical strength. It was shown that, for primary lactose particles to be conserved in spray drying, the dissolved lactose mass loading X_d must be below 5.2%.

© 2017 Elsevier B.V. All rights reserved.

1. Introduction

Spray drying is a widely used technique transforming an atomized liquid feed into dry particles by evaporation of the liquid phase in a gaseous drying medium [1]. The technique is used for heat-sensitive products, such as food and pharmaceuticals, since the temperature of the drying liquid remains below the wet-bulb temperature [2]. A big advantage of spray drying is that drying of emulsions, slurries or pastes may be carried out in one unit operation [3]. Independent of the feed composition, production of spray dried powders with a narrow particle

size distribution requires consistent droplet size formation. In general, production of fine droplets yields individual particle drying with reduced tendency for agglomeration during drying.

Single droplet drying and particle formation during spray drying are difficult to investigate, because of the complex two-phase flow in spray dryers and other difficulties as described by Vehring et al. [4]. Therefore, the drying behavior of individual droplets was studied in the literature with various experimental methods of droplet positioning, such as droplets free flying [5], free falling [6], or pending from a capillary or a filament [7,8]. Other techniques trap droplets on a concave hot plate [9] or freely levitate them using optical, acoustic or electrodynamic forces [10,11]. An acoustic levitator generates a standing acoustic wave with equally spaced pressure nodes and a corresponding quasi-steady pressure distribution allowing individual droplets to be levitated. Investigations of the progression of drying with this technique were successful for droplets of liquid mixtures [12], aqueous solutions [13] and aqueous suspensions [14]. The drying of droplets in an acoustic

Abbreviations: API, active pharmaceutical ingredient; ASTM, American Society for Testing and Materials; CCD, charge-coupled device; DSA, density and sound velocity apparatus; PSD, particle size distribution; RSD, relative standard deviation; SCS, side crushing strength; VWR, Van Waters & Rogers.

* Corresponding author at: Research Center Pharmaceutical Engineering (RCPE) GmbH, 8010 Graz, Austria.

E-mail address: khinast@tugraz.at (J.G. Khinast).

Nomenclature

A	decreasing droplet surface area of an oblate spheroid/m ²
A_0	initial droplet surface area of an oblate spheroid/m ²
$A_{s,o}$	droplet surface area of an oblate spheroid/m ²
m	mass of droplet/g
m_d	mass of dissolved lactose/g
m_{H_2O}	mass of water/g
m_l	mass of isopropanol/g
m_{liq}	mass of liquids/g
m_s	mass of suspended lactose/g
m_{solid}	mass of dissolved and suspended lactose/g
q_3^*	particle size density distribution
Re	Reynolds number
t_d	drying time in levitator/min
w_d	dissolved lactose mass fraction/%
w_{H_2O}	water mass fraction in solvent mixture/%
w_s	suspended solid mass fraction/%
w_{solid}	dissolved and suspended solid mass fraction/%
X_d	dissolved lactose mass loading/%
X_L	dissolved lactose mass loading in isopropanol-water mixtures/%
$X_{L,S}$	solubility of lactose in isopropanol-water mixtures/%
ρ_s	density of suspension/g·cm ⁻³
ρ_{sol}	density of solution/g·cm ⁻³

levitator is similar to the process in a spray dryer, as described by Schiffer [15]. One limitation in an acoustic levitator is the droplet size, which is determined by wavelengths between 2.2 and 0.34 cm for ultrasound frequencies between 15 and 100 kHz [16]. Furthermore, the maximum droplet volume and mass for acoustic levitation are limited by the liquid surface tension against the ambient air and the liquid density [17,18]. Typical densities of suspensions for acoustic levitation experiments range between 0.5 and 8 g/ml [19].

Drying may be enhanced by convection through a gas flow, but independent of that the droplet undergoes two drying stages until a final dry particle is formed. The first drying stage is known as the constant-rate period, since the surface of the droplet decreases at a constant rate due to evaporation of the liquid from the surface. This drying stage therefore follows the so-called d^2 law [20]. Suspension droplets exhibit this behavior as long as the surface is wetted [21]. The mass loss of the liquid leads to an increase of the solid mass fraction in the droplet. At high ratios of droplet-shrinkage-rate-to-diffusivity in the liquid phase, a non-uniform radial distribution of the solid may arise, leading to crust formation [14]. These phenomena may further influence the evaporation rate and, consequently, the duration of the first and the second drying stages. Different mechanisms of heat and mass transport may occur inside the microsphere (transport of liquid and liquid vapor, heat transfer, migration of the liquid surface into the microsphere). The local porosity of the solid, surface roughness and solids distribution inside the microsphere may result in a highly complex evolution of the second drying stage [14].

In the course of the first drying stage, the solid fraction of the droplet increases due to evaporation of the liquid. The end of the first drying stage is defined by the rise of the droplet temperature above wet-bulb level. In the second drying stage, evaporation is reduced by the resistance against liquid transport from the inside of the droplet (which slowly becomes a solid microsphere) to the surface. In this period, volume change due to the shrinkage is negligible. The liquid evaporation results in a loss of mass, which can be detected by a change of the microsphere position in the acoustic levitator. As the microsphere loses weight, it moves upward towards the nearest pressure node. The remaining liquid may evaporate inside the porous structure rather than on the most outer surface. Solids dissolved in the liquid may

precipitate on the way to the surface or on the surface, resulting in a dense packing of the primary particles of the suspension or the formation of a completely closed solid layer on the surface.

The drying of pure liquid [12,22], solution [23,24] and suspension droplets [21,25] was investigated in the literature. Drying of suspension droplets with dissolved solids, however, has been studied to a much lesser extent. A better understanding of the drying of suspension droplets is needed to evaluate the influence of the suspension composition on the dried particle properties. Knowing the influencing factors during spray drying of suspensions will make it possible to choose process parameters during drying which avoid change of particle properties. This is an advantage in manufacturing of API.

In a pharmaceutical continuous manufacturing process, drying is one of the last unit operations of primary manufacturing, before entering processes further downstream (secondary manufacturing), such as blending, granulation, tableting or capsule filling [26]. Looking at this process from the beginning, production starts with the synthesis of the API and continues with crystallization. Afterwards, several washing [27] and filtration [28,29] steps are needed to obtain a purified solid drug product. The purification steps are vital to remove impurities. Finally, the drug crystals are dried [30,31] where care has to be taken to avoid major changes of final powder properties, such as the particle size distribution. If the carrier liquid of the suspension to be dried contains significant amounts of dissolved solids, agglomeration of primary particles by precipitated solids is likely to occur. The amount of dissolved solids (and thus, of the solid bridges) will then determine the mechanical strength of a dried agglomerate. If the connections (solid bridges) between primary particles are weak enough, the primary particles can be obtained by break-up of the agglomerates due to low-grade mechanical forces.

For this reason, there is interest in characterizing material's mechanical properties of spray-dried pharmaceutical microspheres. Methods characterizing the bulk properties of powders, such as the bulk density, the cohesive strength, the angle of repose and other parameters do not reveal information about individual particles [32]. In contrast to this, recently developed methods assess the individual particles by micro- and nano-indentation techniques [33–36]. Mechanical properties of individual particles, such as the hardness, the elastic modulus, the stiffness, or the load displacement curves, are determined by atomic force microscopy nano-indentation experiments [37–41]. Transferring the results from microscopic single particle measurements to a macroscopic level, however, is difficult. Some attempts were recently made to assess the mechanical strength of individual or agglomerated particles of ceramics [42], catalyst carriers [43] and calcium carbonate granules [44–47].

In the present work we studied the evaporation kinetics of suspension droplets, with solids dissolved in various carrier liquids, and the resulting microsphere morphology of pharmaceutical excipients. Furthermore, the mechanical properties of individual microspheres were evaluated by hardness measurements and related to the solid's solubility in the liquid. Our hypothesis is that the more solid material is dissolved in the liquid, the stronger solid bridges (obtained upon drying) will be, increasing the mechanical strength of the microspheres.

2. Materials and methods

2.1. Materials

Lactose GranuLac® 230 was obtained from Molkerei Meggle Wasserburg (Wasserburg, Germany) with a particle size distribution (PSD) as shown in Fig. 1 and particle shapes as shown in Fig. 2. Water of analytical grade was produced with an Ultrapure Water System from TKA (Niederelbert, Germany). Isopropanol in high purity ($\geq 99.8\%$) was obtained from Carl Roth (Karlsruhe, Germany).

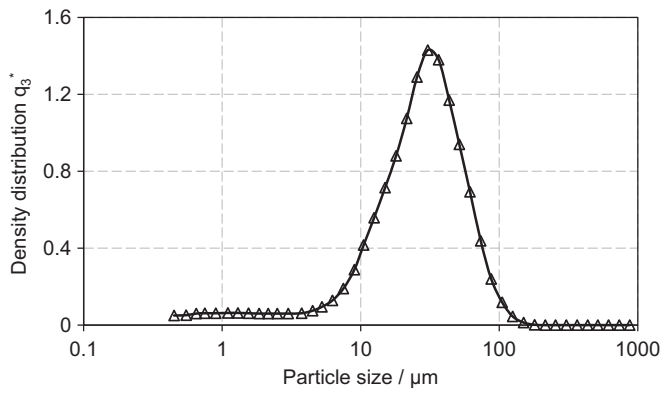


Fig. 1. Particle size distribution of raw material GranuLac® 230.

2.2. Solubility measurements of lactose in isopropanol-water mixtures

The following definitions were chosen, i.e., the mass of the liquid mixture m_{liq} consisting of H_2O and solvent I (isopropanol) in Eq. (1), the water mass fraction w_{H_2O} in Eq. (2) and the solubility of lactose X_L in Eq. (3).

$$m_{liq} = m_{H_2O} + m_I \quad (1)$$

$$w_{H_2O} = \frac{m_{H_2O}}{m_{liq}} \quad (2)$$

$$X_L = \frac{m_d}{m_{liq}} \quad (3)$$

Here m_d is the mass of the dissolved excipient (alpha-lactose monohydrate). Solubility measurements of alpha-lactose monohydrate in different water-isopropanol mixtures were carried out by measuring the solution densities with DSA 5000 M from Anton Paar (Graz, Austria). The measurements were carried out at the constant temperature of 25 °C and covered solvents with five different water mass fraction w_{H_2O} between 40% and 90%.

For determination of the solubility, the densities of the mixtures m_{liq} were measured in the following manner. The density of each isopropanol-water mixture was measured. Afterwards, for each of the mixtures, four solutions with known amounts of dissolved lactose m_d were prepared, as depicted by the square symbols in Fig. 3. All the lactose concentrations were below the saturation concentration. Solid concentrations were increased with increasing water mass fraction w_{H_2O} . For the solution preparation, a known amount of lactose was suspended in the solvent mixture and the suspensions were placed in

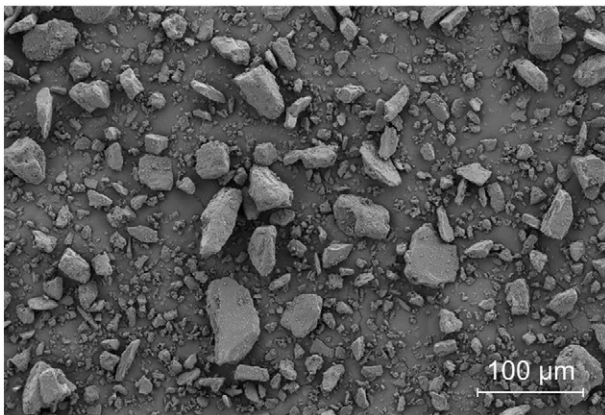


Fig. 2. Scanning electron micrograph of raw material GranuLac® 230.

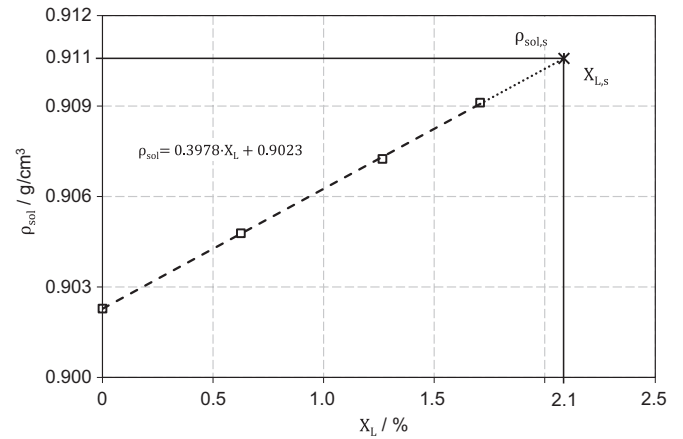


Fig. 3. Determination of the solubility $X_{L,s}$ from different solution densities ρ_{sol} for a water mass fraction w_{H_2O} of 50% at 25 °C. The square symbols represent solution densities ρ_{sol} with known mass of dissolved lactose m_d and the dashed line shows the linear fit curve ρ_{sol} . The dotted line depicts the extrapolation to calculate the solubility $X_{L,s}$ (star symbol) from the measured saturated solution density $\rho_{sol,s}$.

an incubating orbital shaker 3500I from VWR (Pennsylvania, United States) at 25 °C for 24 h. After this time, the lactose was completely dissolved. The density of each solution was measured five times. The RSD of all the measurements was below 0.02%. With these data, a linear relation was obtained for the unsaturated regime between solution densities ρ_{sol} and the dissolved lactose mass loading in isopropanol-water mixtures X_L . The linear relation is depicted in Fig. 3 for a water mass fraction w_{H_2O} of 50%. This procedure was carried out for all water mass fractions w_{H_2O} and enabled the calculation of linear fit curves ρ_{sol} as depicted in Table 1.

To determine the concentration at saturation, saturated lactose solutions were prepared for all the five solvent mixtures. A surplus of lactose was suspended in the liquids, and the mixtures were placed in an orbital shaker at 25 °C for 48 h. The saturated solutions $\rho_{sol,s}$ were decanted and, before measurement, filtered with a syringe filter from Merz Brothers GmbH (Vienna, Austria) with a pore size of 0.22 μm. The concentration of the saturated solutions $\rho_{sol,s}$ was measured five times. The RSD for all the measurements was below 0.02%. The solubility $X_{L,s}$ of the saturated solutions $\rho_{sol,s}$ was calculated from the density using the previously determined linear fit curves ρ_{sol} . The densities $\rho_{sol,s}$ of the saturated pure water and pure isopropanol solutions were not measured to calculate the lactose solubility, because these values were available from the literature [48,49]. Fig. 4 represents the solubility of lactose $X_{L,s}$ in the isopropanol-water mixtures in the form of water mass fractions w_{H_2O} .

2.3. Levitation drying setup

Experiments for assessing the drying kinetics of lactose suspensions with different lactose mass fractions and solvent compositions were carried out using an acoustic levitator. Acoustic levitation is commonly used for studying transport processes with individual objects suitable for being positioned in the quasi-steady pressure field of the resonator. This levitation technique works without mechanical contact between

Table 1

Measured saturation densities $\rho_{sol,s}$ and calculated solubilities $X_{L,s}$ from the linear fit curve ρ_{sol} at different water mass fractions w_{H_2O} .

$w_{H_2O}/\%$	Linear fit curve ρ_{sol}	R^2	$\rho_{sol,s}/g/cm^3$	$X_{L,s}/\%$
40	$0.4637 \cdot X_L + 0.8786$	0.9477	0.883	0.92
50	$0.3978 \cdot X_L + 0.9023$	0.9998	0.911	2.06
60	$0.3906 \cdot X_L + 0.9256$	0.9992	0.941	3.80
80	$0.3769 \cdot X_L + 0.9667$	0.99997	1.005	9.95
90	$0.4007 \cdot X_L + 0.9807$	0.9987	1.041	14.72

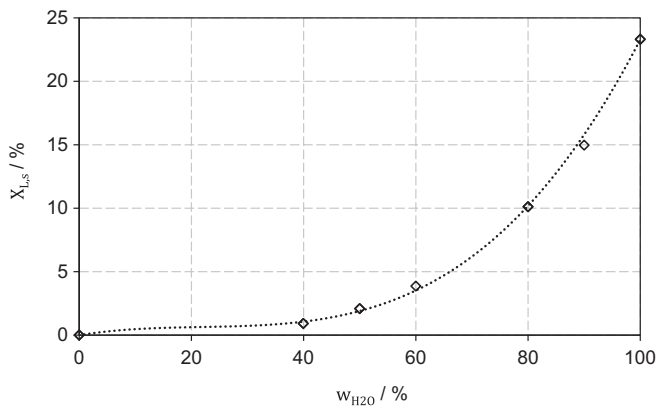


Fig. 4. Solubility $X_{L,S}$ of alpha-lactose monohydrate in isopropanol-water mixtures at 25 °C.

the levitated object and a solid body. Heat and mass transfer from the object are therefore influenced by the acoustic streaming field of the resonator only, and they may be controlled by additional air streams around the object.

The ultrasound transducer of the levitator used in the drying experiments was supplied by tec5 AG (Oberursel, Germany). The experimental setup can be seen in Fig. 5. The standing ultrasound wave is generated by an acoustic resonator consisting of the transducer and a reflector. The vibrating horn of the transducer is made of stainless steel and driven by a piezo-crystal at the frequency of 58 kHz. The interaction of the ultrasound with the reflector produces standing soundwaves with a quasi-steady pressure distribution in the resonator. Proper coaxial relative alignment of the transducer and the reflector allows for a sound-pressure level in the resonator strong enough for levitating the object, and low enough to keep the deformation of the object to a minimum. The presence of the object in the resonator produces a steady acoustic-streaming flow which influences the transport processes from the object. The acoustic streaming vortices, however, rather form a closed flow system in the air around the object and are saturated by the vapor produced by the drying process. To prevent a retarding effect from this vapor content of the vortices, an

additional upward flow of drying air is provided through a hole in the reflector plate. This air flow is provided from the in-house pressurized air system and controlled by a mass flow controller from Bronkhorst (AK Ruurlo, Netherlands).

The temperature in the acoustic levitator during the drying experiments was in the range of 25 ± 2 °C. The drying air flow was set at a velocity of 0.66 m/s, corresponding to a Reynolds number of 170 at the exit hole of the air supply. Additional experiments were carried out without air flow around the droplet for comparison.

The process of droplet drying was recorded using a CCD camera Sony XCD-X710 (Tokyo, Japan) with a CCD chip of 1024×768 pixels. The image resolution was 166 pixels/mm. The CCD camera was used with a macro lens Pentax, 50 mm, 1:2.8 (Tokyo, Japan). The data evaluation of the images was carried out with the public domain software ImageJ, version 1.49, to obtain the surface area of the droplet, the aspect ratio of its shape, and the coordinates of the center of gravity relative to a reference point in space. The droplet surface area of an oblate spheroid $A_{s,o}$ was calculated via Eq. (4) through the half-major (a) and the half-minor (b) axes lengths [50]:

$$A_{s,o} = 2\pi a^2 \left(1 + \frac{b/a}{\sqrt{a^2/b^2 - 1}} \arcsin \sqrt{a^2/b^2 - 1} \right) \quad (4)$$

The raw data were analyzed as functions of time to calculate the droplet surface decay, assuming axial symmetry. The vertical displacement of the droplet due to the mass loss was measured as well. Thus, drying kinetics can be studied also in the second drying stage, where the drop has a constant size and shape. The images were recorded with a frequency between 0.5 and 0.067 Hz, depending on the state of evaporation. Every experiment was repeated five times for each droplet liquid composition.

2.4. Preparation of suspensions and droplet formation

The suspensions investigated consisted of one solid material (lactose) in mixtures of water and isopropanol (or in the pure species) as the carrier liquids. A part of the solid material was dissolved in the

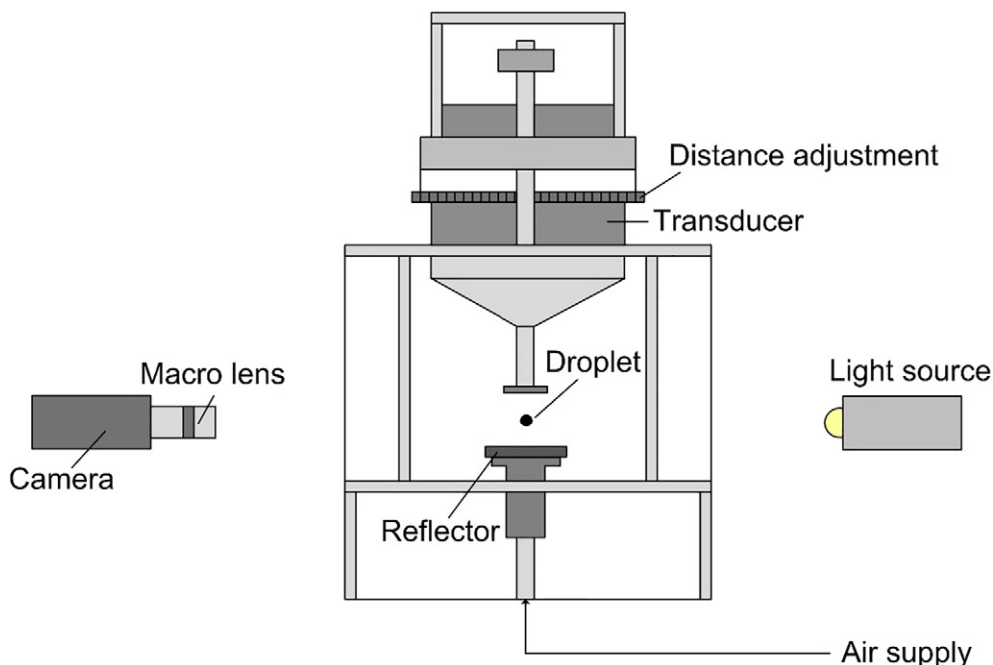


Fig. 5. Ultrasonic levitator and imaging equipment for measuring individual droplet drying kinetics.

liquid, according to its solubility. A droplet with the mass m therefore consists of the dissolved mass m_d and the suspended mass m_s of the solid material in a mixture of the liquid masses m_{H_2O} and m_l of water and isopropanol. We can therefore write

$$m = m_d + m_s + m_{H_2O} + m_l \quad (5)$$

Depending on the water mass fraction w_{H_2O} (Eq. (2)), different mass of solids m_{solid} (Eq. (6)) were present in one suspension droplet. The solids mass m_{solid} consists of dissolved m_d and suspended solids m_s .

$$m_{solid} = m_d + m_s \quad (6)$$

In terms of definition, the mass m was used as reference to define the dissolved solid mass fraction w_d (Eq. (7)), the suspended solid mass fraction w_s (Eq. (8)) and the total solid mass fraction w_{solid} (Eq. (9)).

$$w_d = \frac{m_d}{m} \quad (7)$$

$$w_s = \frac{m_s}{m} \quad (8)$$

$$w_{solid} = \frac{m_{solid}}{m} = w_d + w_s \quad (9)$$

For the preparation of a suspension, a saturated solution of lactose was prepared beforehand as the carrier liquid to avoid changes of the particle size or shape due to dissolution of the lactose. Water and isopropanol were mixed in different ratios in sealable flasks and stirred for 1 h to ensure homogeneous solvent mixtures. Lactose was then added in surplus to the liquids and shaken with an incubating orbital shaker 3500l from VWR (Pennsylvania, United States) for 48 h at 25 °C. The saturated solutions were decanted and filtered with MN 618 from Macherey-Nagel (Düren, Germany). Solid lactose particles were then added to obtain the suspensions. The suspensions were ranked by the dissolved lactose mass loading X_d (Eq. (10)), which is further used as naming convention in the results and discussion part.

$$X_d = \frac{m_d}{m_{solid}} \quad (10)$$

The first three investigated compositions in Table 2 were done in pure isopropanol with variations in the suspended lactose mass fraction w_s from 10% to 50%. Afterwards, the measurement series was continued with the same suspended lactose mass fraction w_s of 10% and varying dissolved lactose mass fractions w_d , ranging from 0.0072% to 17%. These variations are due to different water mass fractions w_{H_2O} , ranging from 0% to 100%. In addition, the water mass fraction w_{H_2O} determined the drying time t_d in the levitator. This time was varied between 10 and 35 min to guarantee complete drying of the microspheres.

Table 2
Compositions of suspensions for drying experiments.

X_d /%	w_d /%	w_s /%	w_{solid} /%	w_{H_2O} /%	$X_{L,s}$ /%	ρ_s /g/cm ³	t_d /min
0.072	0.0072	10	10.01	0	0.008	0.819	10
0.019	0.0056	30	30.01	0	0.008	0.913	10
0.008	0.004	50	50.00	0	0.008	1.031	10
4.00	0.42	10	10.42	10	0.47	0.865	10
5.3	0.56	10	10.56	20	0.62	0.898	10
5.5	0.58	10	10.58	22.5	0.64	0.904	10
5.6	0.60	10	10.60	25	0.67	0.910	15
5.8	0.62	10	10.62	27.5	0.69	0.915	15
6.1	0.65	10	10.65	30	0.73	0.920	15
8.7	0.95	10	10.95	40	1.06	0.935	20
14.4	1.68	10	11.68	50	1.90	0.948	25
34.4	5.25	10	15.25	70	6.19	0.980	30
55.1	12.28	10	22.28	90	15.80	1.048	30
63.0	17.00	10	27.00	100	23.29	1.104	35

At the beginning of the drying experiments, droplets with volumes in the order of 2–3 μ l were inserted into the acoustic field with a microliter syringe from Terumo (Tokyo, Japan). The inserted droplet volumes were slightly different for different suspensions, since releasing a droplet from the syringe with higher suspension solid loadings was only possible with bigger droplets. Thus, larger droplets were obtained for higher solids loadings. This experimental difficulty was described as well by Yarin et al. [21]. However, a uniform initial droplet volume was achieved for a given constant solids loading.

Achieving a consistent solid loading in the levitator droplets is another experimental concern. Thus, the lactose content in the droplets was verified by weighing to ensure that drying starts always at the same initial conditions. For this purpose, droplets were formed with a microliter syringe, inserted in a sealable plastic pipe from Eppendorf (Hamburg, Germany), and weighed before and after drying with an analytical balance XP205 DR from Mettler Toledo (Giessen, Germany). Suspended lactose mass fraction w_s of 10%, 30% and 50% were examined in pure isopropanol as solvent. After droplet insertion, the sealable plastic pipe was closed immediately before weighing, to avoid evaporation of volatile components. Afterwards, the sealable plastic pipe was opened to enable evaporation of volatile components under controlled conditions in a compartment drier from Binder (Tuttlingen, Germany) at 40 °C for 30 min. The mass of dried lactose in a single droplet was calculated and compared with the set solid content in the prepared suspension. Table 3 depicts the results for the measured solid mass fraction in one droplet for lactose isopropanol suspensions.

Scanning electron micrographs of the microspheres were recorded with the Zeiss Ultra 55 from Carl Zeiss AG (Oberkochen, Germany) with an Everhart-Thornley detector and an acceleration voltage of 5 keV. The microspheres were sputtered with the sputter coater EM ACE600 from Leica (Wetzlar, Germany) with a 15 nm gold-platinum (80%–20%) layer to enable good electrical conductivity.

2.5. Hardness measurement setup

The hardness of individual microspheres was measured with the side-crushing-strength (SCS) test in a slightly modified version. This test method is applied to determine the compressive strength of individual particles. In this test, the sample is placed between two platens and compressed by linear movement of one plate [43,51]. An exact procedure for this test method is described in ASTM Standard D4179-01 for crushing of single catalyst pellets [52]. In our work, the agglomeration strength of individual dried microspheres was measured using a rheometer MCR 300 from Anton Paar (Graz, Austria) in the plate-plate configuration with a normal force range from 10 to 5000 mN and a normal force resolution of 5 mN. For this measurement, individual microspheres dried in the acoustic levitator were placed in the center of the bottom plate, and the upper plate was moved downward at the constant velocity of $5 \cdot 10^{-6} \text{ m} \cdot \text{s}^{-1}$ (see Fig. 6). The normal forces were recorded while the upper plate was moving.

Investigations of the mechanical strength of granules produced in continuous granulators were also reported in the literature [44–47]. In these experiments, a minimum of 100 granules were analyzed to obtain statistically reliable results. In our experiments, measurements with such a large numbers of microspheres were not possible. Nevertheless, at least five individual microspheres were crushed for each suspension composition to have statistical information on the results.

Table 3
Set suspended lactose mass fraction w_s in comparison with the measured suspended lactose mass fraction w_s in one droplet for pure isopropanol as solvent.

Set w_s /%	Measured w_s /%	RSD/%
10	10.07	2.8
30	31.19	3.2
50	50.67	4.2

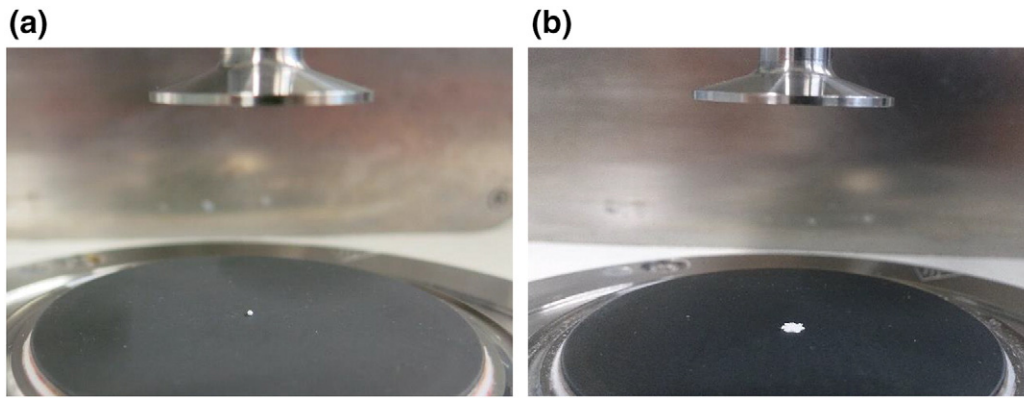


Fig. 6. Microsphere on the rheometer plate (a) before and (b) after hardness test.

3. Results and discussion

3.1. Drying kinetics and morphology of lactose-isopropanol suspensions

The pressure forces from the acoustic field levitating the droplet result in oblate spheroidal droplet shapes [53]. Therefore, the diameter of a sphere cannot be used to track the temporal drying progress in the acoustic field. Thus, drying kinetics were obtained through the surface decrease as described in Section 2.3.

Individual droplet drying experiments with mixtures of lactose and pure isopropanol with a suspended lactose mass fraction w_s of 10%, 30% and 50% were performed at 25 °C without drying air flow. Lactose has a very low solubility in isopropanol. The data from the experiments in Fig. 7 reveal that the first drying stage depends on the solids content. Higher solids content in the droplet resulted in smaller changes of the droplet diameter and, consequently, shorter first drying stages. As long as the droplet surface is wetted with isopropanol, the drying occurs at the same rate for each solids content. This constant-rate period is known as the first drying stage. After its end, the drying continues at constant microsphere volume in the second drying stage. The kinetics of the transition from the first to the second drying stage is similar for each solid content, resulting in similar shapes of the curves in Fig. 7.

Dried particles from these experiments are shown in Fig. 8. As mentioned above, initial droplet size varied with the solids content of the suspension. The larger droplets exhibit more strongly deformed shapes, which can be attributed to a balance of the levitating force from the acoustic field and the droplet weight [54]. An almost spherical droplet (and as result, a spherical microsphere) with an aspect ratio of 1.05 was obtained for a w_s of 10% lactose (Fig. 8a). The aspect ratio increased

to 1.2 for a w_s of 30% lactose (Fig. 8b), and the spheroidal droplet with the highest aspect ratio of 1.5 was observed for the highest w_s value of 50% lactose (Fig. 8c), which had the highest suspension density ρ_s .

The solubility of lactose in isopropanol of 0.008 g/l is very low [49] compared to the solubility in water. The resulting small amount of dissolved solids enables drying of primary particles. Moreover, no significant solid bridges are formed between primary particles upon

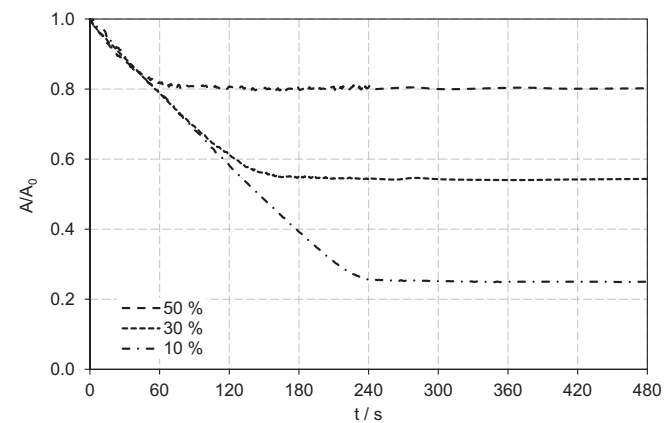


Fig. 7. Drying of lactose-isopropanol suspensions with different suspended lactose mass fractions w_s of 10%, 30% and 50% at ambient air temperature of 25 °C without drying air flow.

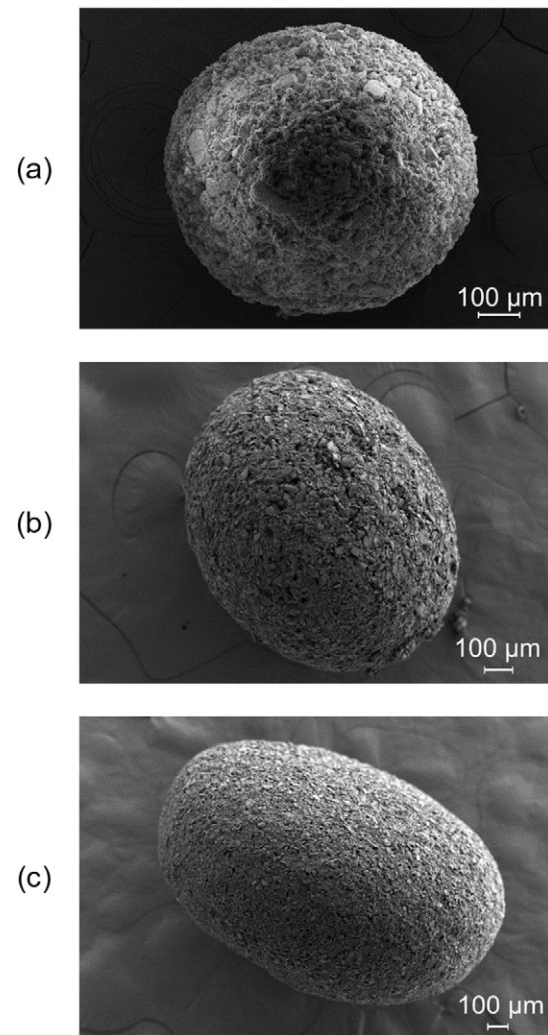


Fig. 8. Scanning electron micrographs of microspheres collected from the levitator after drying at 25 °C. Drying of lactose-isopropanol mixtures with a suspended lactose mass fraction w_s of (a) 10%, (b) 30%, (c) 50%.

drying. For all three cases, the morphologies of the dried microspheres (Fig. 8) were the same. No bonding of primary particles due to precipitated solid bridges was observed for these compositions. Different microsphere sizes were observed for the different solids contents, as seen in Fig. 8. Clearly, initially more dilute suspensions resulted in smaller microspheres than the more concentrated ones due to lower solid contents.

A drying air flow with the volume flow rate-equivalent velocity of 0.66 m/s in the reflector hole reduced the duration of the first drying period for a suspended lactose mass fraction w_s of 10% by a factor of 3, as depicted in Fig. 9. Additionally, drying with air flow resulted in a shorter transition between the first and second drying stages. In contrast to this, drying without air flow revealed a longer transition with a more rounded curve. The differences in the drying kinetics observed are due to the ventilation of the acoustic streaming vortices near the drying droplet. Thus, the reduced vapor content of the vortices allows for the observed higher drying rate. An additional convective influence from the drying air flow on the droplet is not the reason for this effect [15].

3.2. Drying kinetics and morphology of lactose-isopropanol-water suspensions

In this section, individual droplet drying experiments were performed for the fixed suspended lactose mass fraction w_s of 10% and different compositions of the carrier liquid of the suspension. The varying liquid compositions (water mass fractions w_{H_2O} from 0% to 70%) exhibit different solubility of lactose, and therefore, resulted in different dissolved lactose mass loadings X_d from 0.072% to 34.4%. The saturation concentrations of lactose in pure water and in pure isopropanol are 233 g/l and 0.008 g/l, respectively [48,49]. Liquids with higher water content allow for higher dissolved lactose concentrations, as shown in Fig. 4. Furthermore, water reduced the evaporation rate of the suspension carrier liquid, because water is less volatile (pure water vapor pressure at 25 °C is 3.169 kPa [55] than isopropanol (pure isopropanol vapor pressure at 25 °C is 5.846 kPa [56]).

Fig. 10 depicts the drying of individual droplets with the same suspended lactose mass fraction w_s of 10% and different compositions of the carrier liquid. The drying air flow with 0.66 m/s ($Re = 170$) was again applied to control the vapor content of the acoustic streaming vortices.

The drying of an individual droplet consisting of lactose and isopropanol without water revealed the fastest evaporation rate in the first drying stage. Adding water to the droplet liquid reduced the evaporation rate, resulting in a longer first drying stage. Water mass fractions

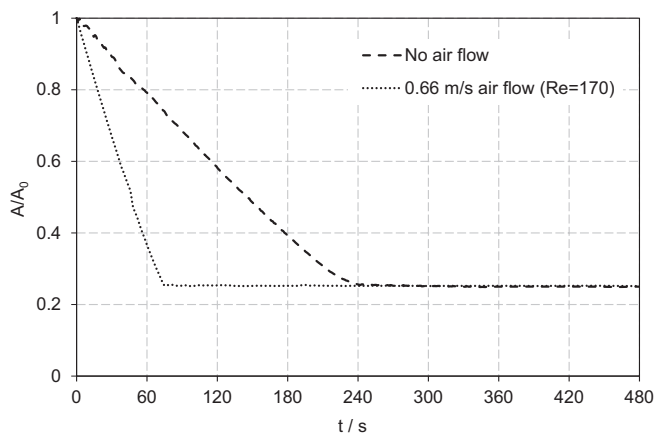


Fig. 9. Drying of lactose-isopropanol suspensions with a suspended lactose mass fraction w_s of 10% at ambient air temperature of 25 °C without and with 0.66 m/s drying air flow.

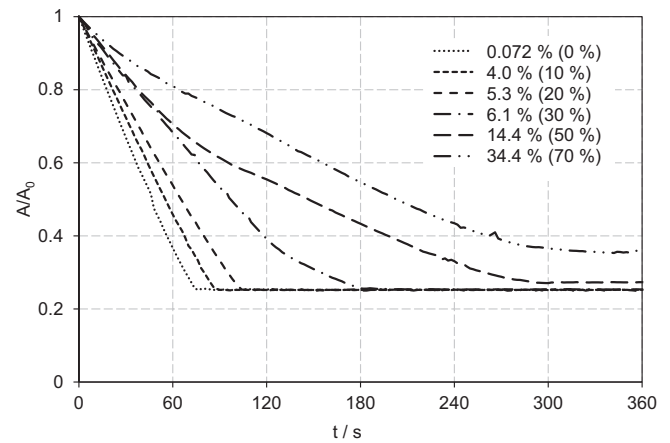


Fig. 10. Drying of lactose suspensions with the same suspended lactose mass fraction w_s of 10% and different dissolved lactose mass loadings X_d between 0.072% and 34.4% (water mass fractions w_{H_2O} between 0% and 70%).

w_{H_2O} up to 20% showed pure liquid drying kinetics and negligible influences of the slower evaporating water. Water mass fractions w_{H_2O} above 20% resulted in a change of the drying kinetics due to higher water mass fractions w_{H_2O} in the liquid mixture. These compositions showed different slopes of the drying kinetics, the first one with a steeper slope and the second one with a lower slope. This indicates that the more volatile component (isopropanol) evaporates preferentially first and afterwards the less volatile component (water) [57,58]. These drying kinetics of binary liquid mixtures are due to the different activities of the two liquid components, which furthermore depend on the composition of the liquid phase.

Another effect that reduces the drying rate at higher amounts of dissolved solid is the formation of bridges and shells. As pointed out above, the amount of dissolved solids increased with the water content of the liquid, resulting in a higher total solid loading in the droplet. The dissolved solids precipitated during the drying process and formed bridges between primary particles or a skin on the surface, which reduced the rate of evaporation of the volatile components [3]. At low concentration, the dissolved solids formed a porous structure allowing for fast solvent evaporation. In contrast to this, high amounts of dissolved solids precipitated at the surface and sealed the pores, hindering the evaporation of the liquids.

The electron micrographs in Fig. 11 depict the surface and bulk morphologies of microspheres dried in the levitator with the constant suspended lactose mass fraction w_s of 10% and different dissolved lactose mass loadings X_d between 5.3% and 34.4%.

For low levels of X_d no significant effects of the dissolved solid could be observed, and primary particles had no visible connections by precipitated material. For example, the structure for a dissolved lactose mass loading X_d of 5.3% (Fig. 11a) was very similar to the one in Fig. 8a for a much lower X_d of 0.072%. However, raising the water mass fraction w_{H_2O} to 30% and, therefore, the dissolved lactose mass loading X_d to 6.1%, resulted in visible connections of the primary particles with precipitated solids on the surface (Fig. 11b(i)). The precipitated mass acts as a binder and “glues” the primary particles together, resulting in a more densely packed network structure. The particle packing at the droplet surface becomes more intense as the dissolved lactose mass loading X_d increases to 14.4% (Fig. 11c(i)). An additional increase of X_d can even lead to full covering of the microsphere surface with precipitated solids (Fig. 11d(i)). At the dissolved lactose mass loading X_d of 34.4%, no primary particles were visible any more.

In addition to the skin on the microsphere, another effect on the microsphere shape occurred at high dissolved lactose mass loadings X_d : the spherical shape was lost from the dissolved lactose mass loading X_d of 14.4% on, resulting in an ellipsoidal microsphere shape

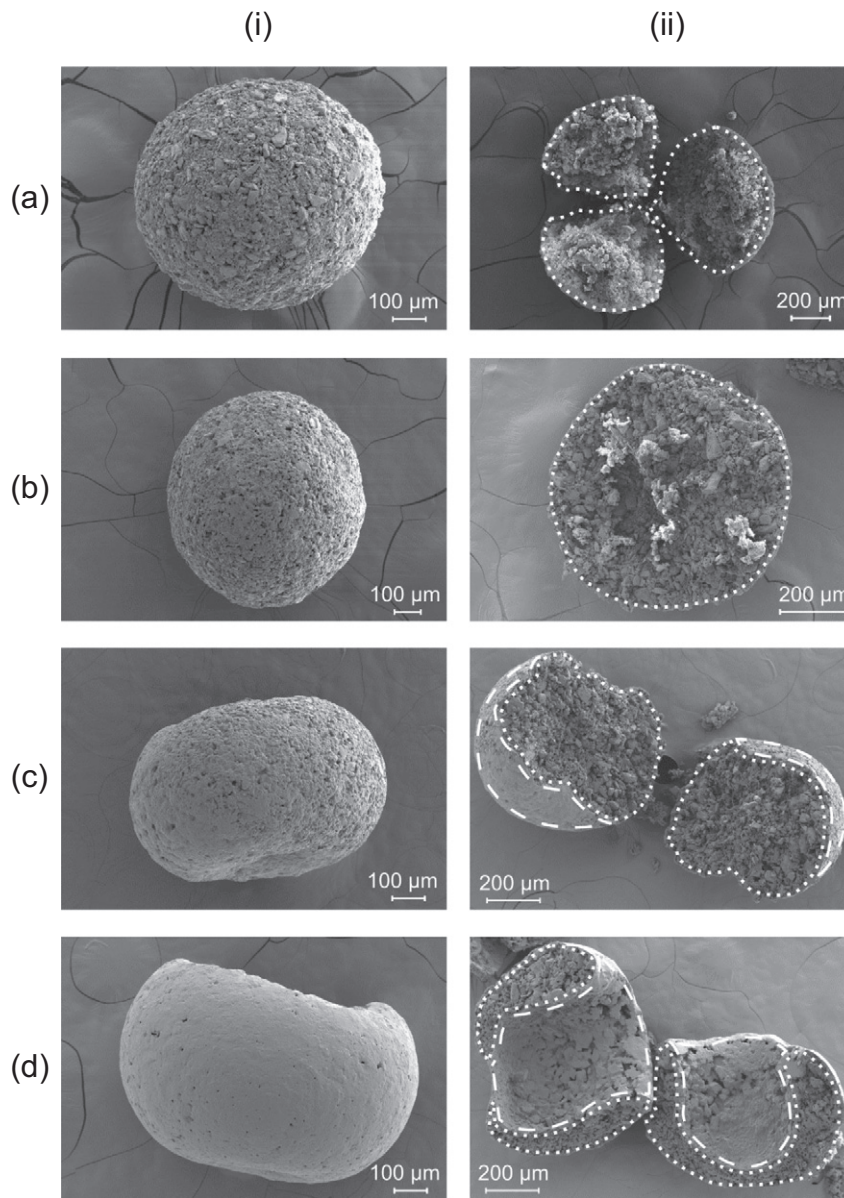


Fig. 11. Scanning electron micrographs of microspheres collected from the levitator after drying at 25 °C with 0.66 m/s air flow. Drying of lactose isopropanol-water mixtures with the suspended lactose mass fraction w_s of 0.1. Left column (i) shows the surface, and right column (ii) the inside structure (area enclosed by dotted line) and the surface (indicated by dashed line) of the microspheres. The dissolved lactose mass loadings X_d and the water mass fractions w_{H_2O} in brackets are (a) 5.3% (20%), (b) 6.1% (30%), (c) 14.4% (50%) and (d) 34.4% (70%).

(Fig. 11c(i)). The reasons for this change of shape are maybe twofold: First, high dissolved lactose mass loadings X_d resulted in high droplet densities and higher mass of the drying droplet. The weight of the droplet was too high to maintain a spherical shape by the levitation force. Second, higher dissolved lactose mass loadings X_d resulted in more precipitated mass, resulting in an unevenly distributed precipitated mass around the droplet. This can even lead to the collapse of the microsphere due to high concentration gradients, resulting in the formation of hollow microspheres (Fig. 11d(i)). This highly concentrated surface leads to an increased viscosity with subsequent crust formation. Remaining solvents can evaporate through pores in the formed crust. Afterwards, the hollow microsphere may collapse, depending on the mechanical properties of the crust [59].

It is known for spray drying of suspensions that during the drying process diffusion of the liquid phase from the core to the surface can lead to voids in the particle. Similar effects have been attributed to the liquid drawn to the surface by capillary forces. Thus a pressure

difference across the droplet surface is formed, resulting in a collapse of the formed microsphere [60,61].

Further information on the inside structure of the microsphere was obtained by electron micrographs of crushed microspheres. At low dissolved lactose mass loading X_d of 5.3%, as in Fig. 11a(ii), no crust was formed on the surface and no solids precipitated inside the particle, resulting in a loosely packed microsphere. Variations in the composition of the suspension to a higher dissolved lactose mass loading X_d of 6.1% altered the microsphere surface towards a more densely packed structure, since more primary particles were connected by precipitated material (Fig. 11b(ii)). Most of the dissolved solids precipitated on the surface. Therefore, a minor proportion precipitated inside the microsphere. Further increase of the dissolved lactose mass loading X_d resulted in the formation of a thicker crust and additional precipitation of material inside the microsphere. This can be clearly seen in Fig. 11c(ii) ($X_d = 14.4\%$) and Fig. 11d(ii) ($X_d = 34.4\%$), where larger agglomerates are visible throughout the cross section.

Fig. 12 shows the particulate structure of the dried microspheres at higher magnification of the surface and the inside, showing clearly the relation between increased dissolved solids and a more coherent and less porous crust.

Comparing the results from microscopy and drying kinetics revealed deviations of drying curves for different compositions of the suspension. Similar progression of the drying curves (almost linear) were obtained up to a dissolved lactose mass loading X_d of 5.3%, as depicted in Fig. 10. A more curved progression was observed for a dissolved lactose mass loading X_d of 6.1% and above, as previously described. Increasing the dissolved lactose mass loading X_d to 14.4% or beyond causes a stronger deviation of the drying curve, as the microsphere shape changed from a solid sphere to a hollow ellipsoid.

The formation of the first connecting solid bridges between primary particles was studied in more detail. This analysis was carried out by raising the water mass fraction w_{H_2O} in steps of 2.5% from 20% to 30%. Fig. 13 reveals clearly that increased water mass fractions w_{H_2O} , and

therefore higher dissolved lactose mass loadings X_d , lead to longer drying times. Although longer drying times were observed for higher dissolved lactose mass loadings X_d , no visual differences were observed as depicted in the electron micrographs of Fig. 14. The microsphere surface, as well as the crushed microsphere, showed no clear connections between primary particles. Nevertheless, the hardness measurements in Section 3.4 show measurable differences in the dissolved lactose mass loadings X_d of the microspheres.

3.3. Relevance of suspension drying kinetics for industrial spray drying process design

In addition to the analysis of the first drying stage, the second drying stage was investigated by evaluation of the vertical position of a droplet in the acoustic field. The drying droplet moves upward in the acoustic field as it loses mass due to the drying. This additional data $z-z_0$, with the initial droplet position z_0 , enabled a complete analysis of both the

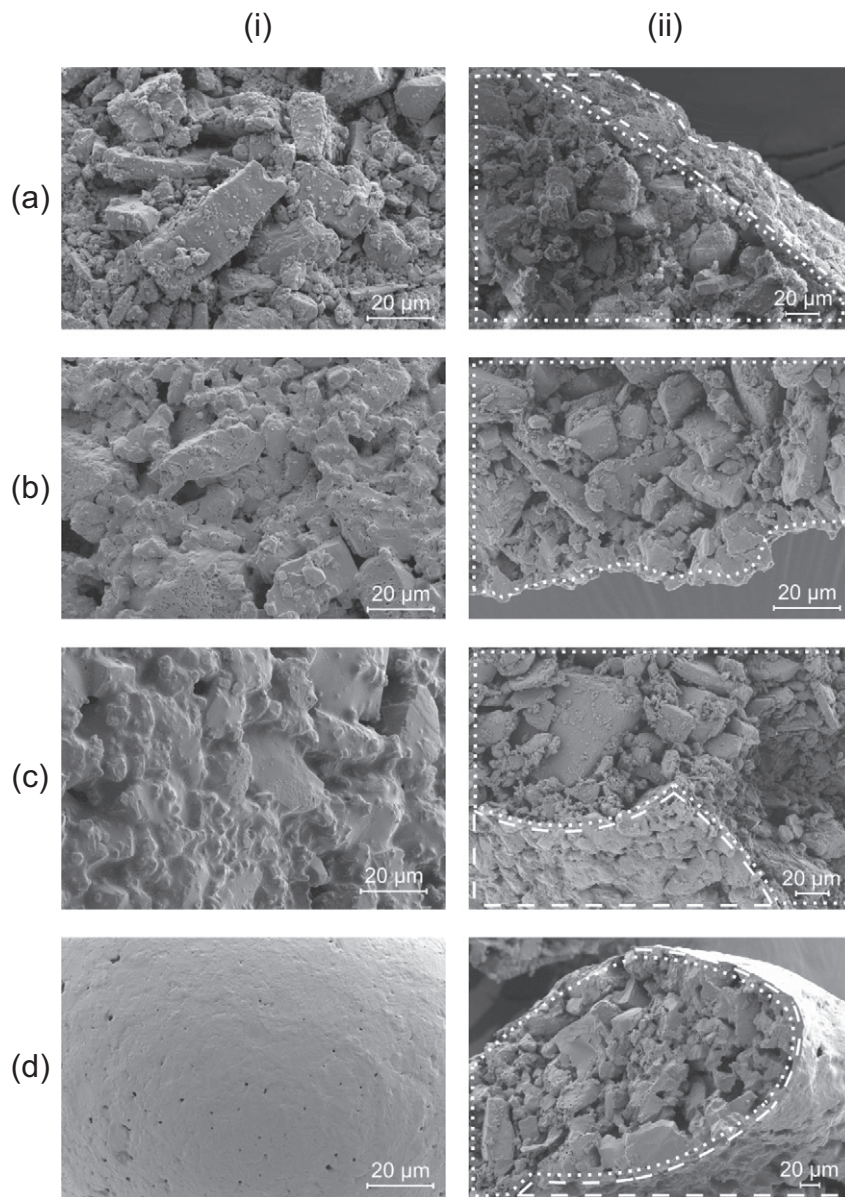


Fig. 12. Scanning electron micrographs of microspheres collected from the levitator after drying at 25 °C with 0.66 m/s air flow. Drying of lactose isopropanol-water mixtures with the suspended lactose mass fraction w_s of 10%. Left column (i) shows the surface, and right column (ii) the inside structure (area enclosed by dotted line) and the surface (indicated by dashed line) of the microspheres at higher magnification. The dissolved lactose mass loadings X_d and the water mass fractions w_{H_2O} in brackets are (a) 5.3% (20%), (b) 6.1% (30%), (c) 14.4% (50%) and (d) 34.4% (70%).

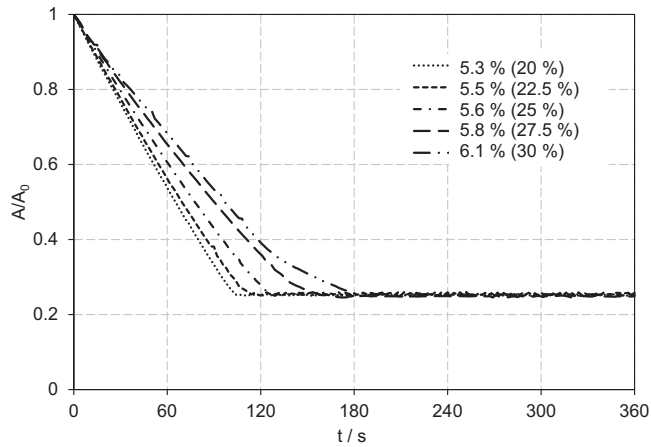


Fig. 13. Drying of lactose suspensions with the suspended lactose mass fraction w_s of 10%, but different dissolved lactose mass loadings X_d between 5.3% and 6.1%. Water mass fractions w_{H_2O} between 20% and 30% shown in brackets.

first and the second stages of the drying process. Fig. 15 depicts the droplet drying kinetics for a suspended lactose mass fraction w_s of 10% and the dissolved lactose mass loading X_d varying from 0.072% to 34.4% due to different liquid compositions.

Drying lactose suspension droplets with pure isopropanol as the solvent (Fig. 15a) show a sharp transition between the first and second

drying periods since the solvent is a pure substance with a high volatility. The droplet moves upward during the whole drying process, and it continues to do so after the end of the first drying period, where the droplet shape and surface remain constant with time, but the droplet still loses mass due to solvent transport through the solid microsphere surface. The second drying stage ends 7 s after the end of the first drying stage. The vertical position of the droplet remains constant after that. An increase of the solvent composition to the water mass fraction w_{H_2O} of 10% reveals a similar drying profile, as shown in Fig. 15b. The influence of the water content on the drying kinetics becomes more apparent at higher amounts, leading to a longer duration of the first and second drying periods and a stronger change of the vertical position. The latter was a result of the larger mass loss of the droplets due to the water evaporation with higher water mass fractions w_{H_2O} .

The shapes of the normalized droplet surface profiles show a significant change in shape as the water content (and thus, the dissolved solid mass) is increased. For water mass fractions w_{H_2O} of 30% and above, a significant change of slope of the droplet surface profiles occurs, the drying kinetics start to become impacted by significant crust formation, leading even to the formation of hollow spheres for even higher water mass fractions w_{H_2O} . Interestingly, the onset of the secondary drying stage, signified by another increase of the droplet position after a steady phase, is delayed for higher water mass fractions w_{H_2O} , likely due to the formation of a significant crust. Apparently, after crust formation, solvent is captured inside the droplet and has to form channels for transport to the outer surface.

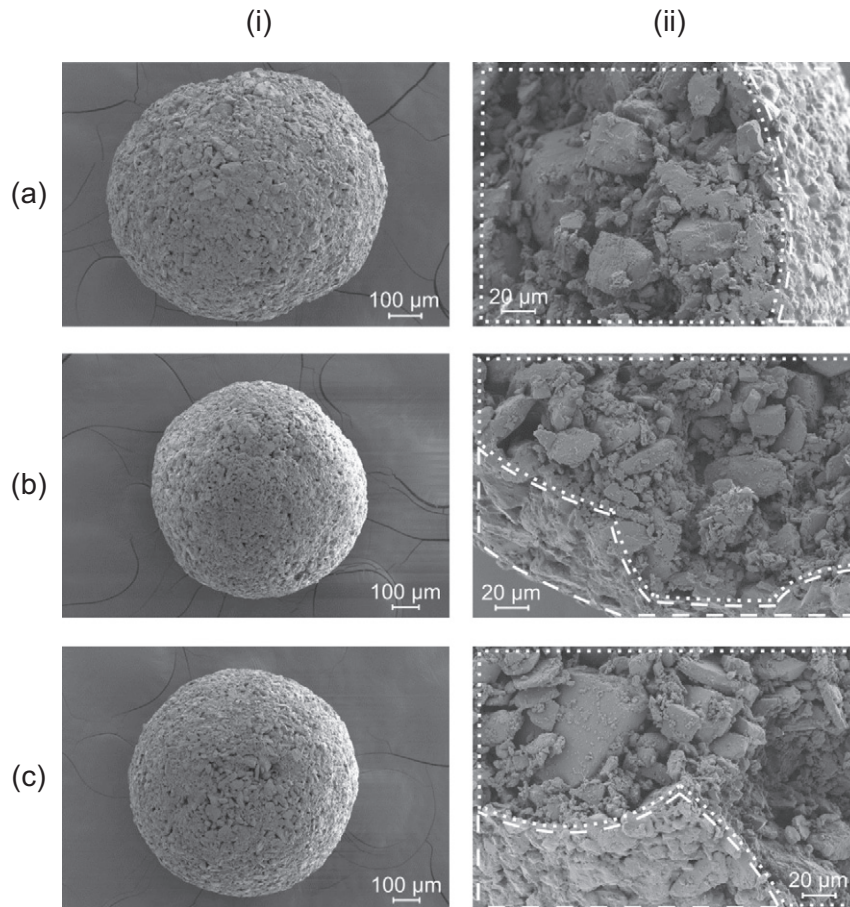


Fig. 14. Scanning electron micrographs of microspheres collected from the levitator after drying at 25 °C with 0.66 m/s air flow. Drying of lactose isopropanol-water mixtures with the suspended lactose mass fraction w_s of 10%. Left column (i) shows the surface, and right column (ii) shows the inside structure (area enclosed by dotted line) and the surface (indicated by dashed line) of the microspheres. The dissolved lactose mass loadings X_d and the water mass fractions w_{H_2O} in brackets are (a) 5.5% (22.5%), (b) 5.6% (25%) and (c) 5.8% (27.5%).

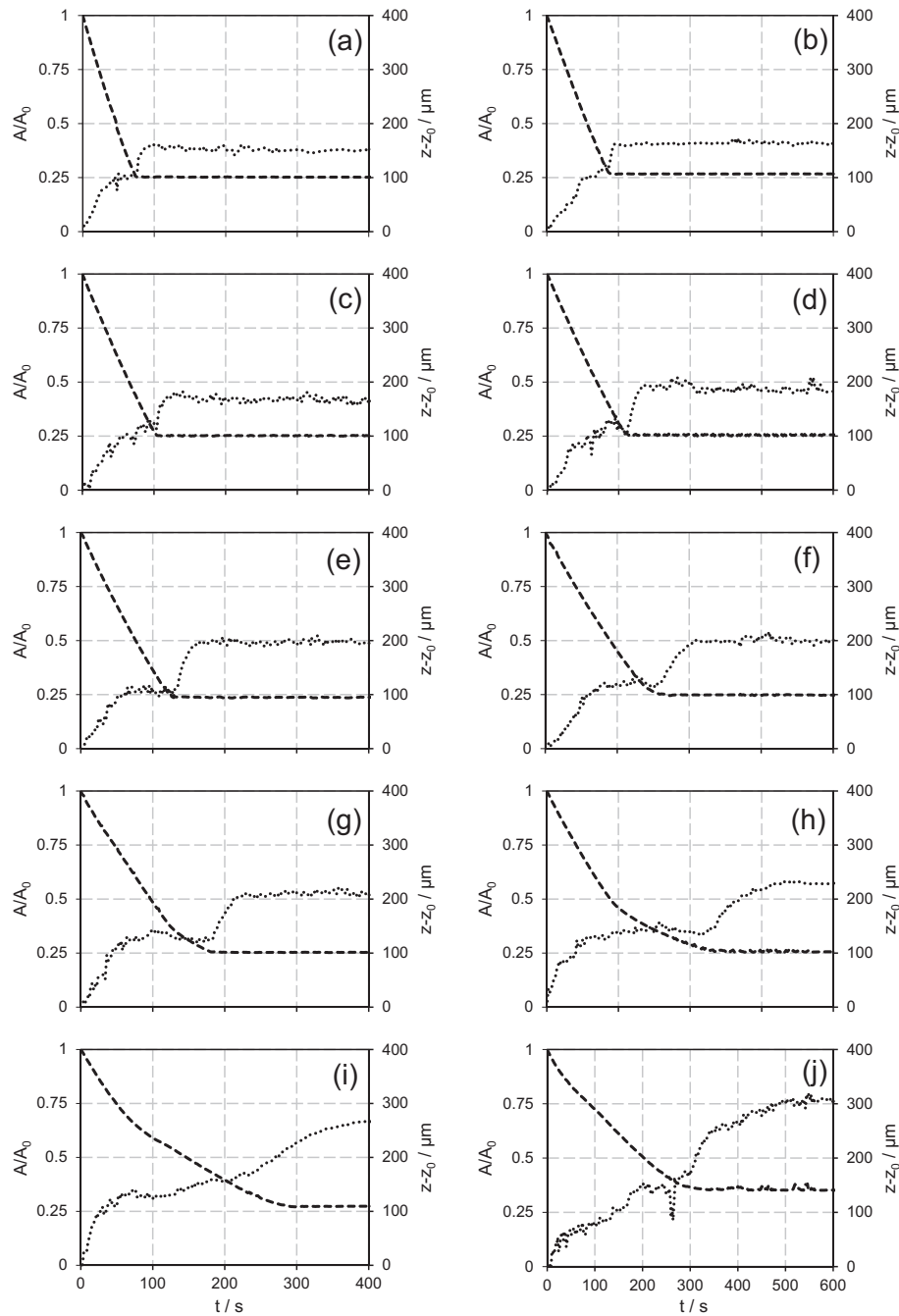


Fig. 15. Drying of individual lactose suspension droplets with the suspended lactose mass fraction w_s of 10% and ten different dissolved lactose mass loadings X_d between 0.072% and 34.4% (water mass fractions w_{H_2O} between 0% and 70%). The dashed lines depict the evolution of the normalized droplet surface, the dotted lines the vertical droplet position in the acoustic field. The dissolved lactose mass loadings X_d and the water mass fractions w_{H_2O} in brackets are (a) 0.072% (0%), (b) 4.0% (10%), (c) 5.3% (20%), (d) 5.5% (22.5%), (e) 5.6% (25%), (f) 5.8% (27.5%), (g) 6.1% (30%), (h) 8.7% (40%), (i) 14.4% (50%) and (j) 34.4% (70%).

Table 4 depicts the durations of the first (normalized droplet area reaches steady state) and second drying periods (height curve reaches steady state) and the changes of vertical droplet position relative to the initial state during drying. These relations between suspension composition and drying time are important for the spray drying process. Suspensions with higher dissolved solids contents or lower rate of solvent evaporation require longer drying times and the primary drying stage (after which shape does not change anymore) is longer as well [62]. Thus, the time to obtain mechanically stable microspheres (which still are wet) is increased: Mechanically of the suspension composition from a dissolved lactose mass loading X_d of 0.072% (water mass fraction w_{H_2O} of 0%) to 8.7% (0.4 40%) resulted in a three times longer

first and a 16 times longer second drying stage. Thus, also the relative duration of the second drying stage increased compared to the primary one.

Further increase of the dissolved lactose mass loading X_d to 14.4% and 34.4% resulted in the formation of solid or hollow ellipsoidal microspheres (Fig. 11c and d), possibly due to stronger concentrations gradients of precipitated solids in the crust. Thus, a collapse of the microspheres was observed (hollow ellipsoidal shape) and the temporal tracking of the surface via backlight images took these indentations (Fig. 11c) or hollow voids (Fig. 11d) not into account (backlight images may show larger surfaces as in reality). Therefore, the drying kinetics for dissolved lactose mass loadings X_d of 14.4% (Fig. 15i) and 34.4%

Table 4

Duration of first and second drying stages and rise $z-z_0$ of the droplet in the acoustic field in the first and second drying stages for the initial suspended lactose mass fraction w_s of 10% and dissolved lactose mass loadings X_d varying between 0.072% and 34.4%.

X_d /%	w_{H_2O} /%	Duration of first drying period/s	Duration of second drying period/s	$z-z_0$ first drying period/ μm	$z-z_0$ second drying period/ μm
0.072	0	76	7	108	41
4.0	10	86	8	113	46
5.3	20	102	24	116	59
5.5	22.5	115	26	117	66
5.6	25	129	36	118	74
5.8	27.5	152	44	120	80
6.1	30	178	50	123	86
8.7	40	220	112	135	95
14.4	50	292	104	167	99
34.4	70	322	218	163	140

(Fig. 15j) differed: First, the onset of the secondary drying stage was delayed for an X_d of 14.4%, whereas the delay was diminished for an X_d of 34.4%. Secondly, the surface ratio of A/A_0 was increased from 0.27 for an X_d of 14.4% to 0.35 for an X_d of 34.4%. The reason for this could be the increased crust of the microspheres and the change from a full microsphere structure to a hollow microsphere with voids. Nevertheless, the results emphasize the trend of prolonged drying times for higher dissolved lactose mass loadings X_d as well as higher water mass fractions w_{H_2O} .

Clearly, drying of such suspensions in a spray dryer will be faster under elevated temperatures and higher drying gas flow rates. Nevertheless, similar effects as the ones observed in our study will be prevalent, and the suspension composition is apparently an important parameter in the design of a spray drying process.

3.4. Mechanical strength of the microspheres

We present a new approach for quantifying the mechanical strength of individual microspheres produced by drying in the acoustic levitator. The method of measuring the mechanical strength was introduced in Section 2.5. Fig. 16 depicts characteristic profiles of the normal force on individual particles, produced and measured by the rheometric device. The independent variable is the displacement of the upper plate of the rheometer. The starting position of the upper plate is at the distance of 750 μm from the bottom plate, and the measurement is stopped at the distance of 500 μm to avoid damages to the equipment. The first change in the normal force is observed as the upper plate takes

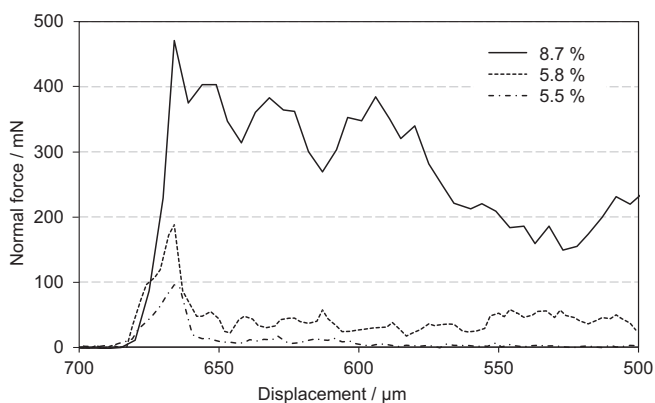


Fig. 16. Normal force on individual microspheres dried in the acoustic levitator as a function of plate distance. The normal force is applied and recorded by a rheometer. The suspended lactose mass fraction w_s was 10%. The dissolved lactose mass loading X_d varied between 5.5% and 8.7%.

up contact with the microsphere. This contact point indicates a typical dimension of the microsphere of 685 μm . Thereafter, the normal force increases rapidly until a maximum force is reached, which indicates the force needed for breaking the microsphere and, therefore, the mechanical strength of the object against normal stress. As the microsphere breaks, the recorded force decreases immediately. Further linear motion of the upper plate leads to normal forces due to the compression of the fragmented microsphere.

Fig. 16 depicts this force for different initial compositions of the suspension. The small dissolved lactose mass loading X_d of 5.5% results in a low breaking force of 101 mN. Increased water content, and therefore, higher dissolved lactose mass loading X_d of 5.8%, results in a higher breaking force of 176 mN. This behavior continues with a further increase of the dissolved lactose mass loading X_d to 8.7%, resulting in an even higher breaking force of 466 mN. Different normal forces are observed for the fragments as well, after breaking of the microsphere, indicating the strength of connections between primary particles. These fragments are weakly connected for a low dissolved lactose mass loading X_d of 5.5%, resulting in low normal crushing forces close to zero. In contrast, higher normal forces are obtained for the fragments for higher dissolved lactose mass loadings X_d .

Tests of the microsphere mechanical strength for the measurement series in Table 2 reveal a strong dependence of the breaking force on the amount of dissolved solids. Due to limitations of the force measurement accuracy, the breaking force could not be recorded for dissolved lactose mass loadings X_d below 4%.

The first measurable breaking force was obtained for the dissolved lactose mass loading X_d of 5.3%, as depicted in Fig. 17a. Small changes in the dissolved lactose mass loadings X_d from 5.5% to 6.1% resulted in an increase of the breaking force. This increase can be explained by inspection of the micrographs in Figs. 11b and 14. More dissolved solids connected the primary particles, resulting in stronger bonds and a significant increase of the breaking force within this transition zone. Increasing dissolved lactose mass loading X_d up to 6.1% resulted in the formation of stronger agglomerates between primary particles, revealing a stronger increase of the breaking force.

At the dissolved lactose mass loading X_d of 14.4%, the measurement method reaches its limitations due to changes of the particle morphology. As depicted in Fig. 11c, the spherical shape is lost and ellipsoidal microspheres are formed. The stress distribution in an ellipsoidal microsphere under normal force is different from a spherical body. This deviation of the shape may be responsible for the higher standard deviation. However, it is clear that stronger microspheres with higher breaking forces are formed at higher dissolved lactose mass loadings X_d . Above a dissolved lactose mass loading X_d of 14.4%, hollow ellipsoidal microspheres are formed, resulting in largely different breaking forces.

The change of the breaking force with variation of the suspension composition is illustrated in Fig. 17a. The transition zone of the dissolved lactose mass loading X_d between 5.5% and 6.1% revealed a non-linear dependency of the breaking force on the dissolved lactose mass content. This effect may be explained by the gradual filling of the voids between primary particles with precipitated solids, resulting in a more densely packed structure, and therefore, higher mechanical strength against normal force. A further increase of dissolved solids content formed a denser packed crust around the microsphere with the effect of a linear relation between higher dissolved lactose mass loadings X_d and maximum breaking forces. The same relation is observed by depicting the breaking force as a function of the water mass fraction w_{H_2O} in the suspension, as in Fig. 17b.

Based on these data, by extrapolation the point was calculated where no force is needed to break the microsphere. This point reflects a suspension composition with a dissolved lactose mass loading X_d of 5.2% or, equivalently, a water mass fraction w_{H_2O} of 19%. This corresponds to our observation that quite loose microspheres are formed below these values. Microspheres from drying of suspensions with

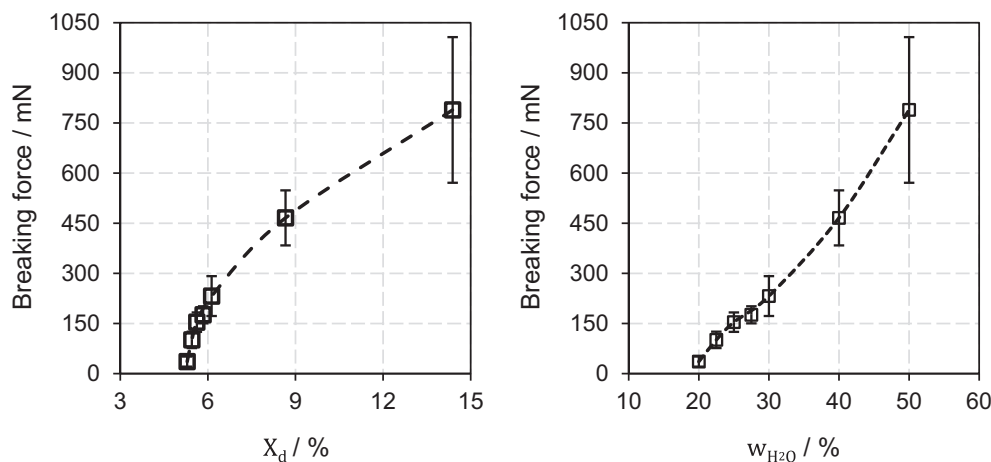


Fig. 17. The breaking force as a function of (a) the dissolved lactose mass loading X_d and (b) the water mass fraction w_{H_2O} .

dissolved lactose mass loadings X_d between 0.072% and 4.0% broke during collection from the acoustic levitator.

These results demonstrate the strong influence of the suspension composition on the mechanical strength of spray-dried particles. There exists a threshold value of the dissolved lactose loading X_d below which loose microspheres are formed. Primary particles are then loosely bonded by precipitated solids, so that the microspheres easily break up, even by weak forces.

4. Conclusions

The present work investigates the influence of initial suspension droplet composition on the drying kinetics via acoustic levitation and the resulting microsphere properties in relation to spray drying. Single droplet drying experiments of a model substance consisting of lactose particles suspended in saturated isopropanol-water lactose solutions were studied at different lactose solubilities. It is found that the dissolved lactose mass loading X_d , which depends on the initial solvent composition, determines the drying kinetics and has a strong influence on the dried microsphere morphology and mechanical strength. The individual microsphere structure changes from loosely packed primary particles with isopropanol as the solvent to denser packing with increasing water mass fraction w_{H_2O} . The dissolved solids precipitate during drying and bond the primary particles. Most of the precipitation occurs at the droplet surface and forms a crust.

The hardness of individual microspheres was measured by a compression strength test. These measurements enabled the mechanical strength of individual microspheres against normal forces to be quantified. Loosely agglomerated microspheres were formed below the threshold $X_d = 5.2\%$ for the investigated model substance. Based on these findings, drying should be carried out below this threshold to enable drying either of primary particles (i.e. tailored particle properties after crystallization remain unaltered during drying), or above this threshold to produce larger, agglomerated particles (i.e. improved powder flowability as favored in direct compression). In conclusion, transferring the results from small scale droplet studies to spray drying emphasizes the importance of fine atomization (small droplets with small amounts of suspended and dissolved solids) of the suspension to produce powders of primary particles mainly. Based on the experimental data presented here, modeling of the dry microsphere formation is underway.

Acknowledgements

This work has been funded within the Austrian COMET Program under the auspices of the Austrian Federal Ministry of Transport,

Innovation and Technology (BMVIT), the Austrian Federal Ministry of Economy, Family and Youth (BMWFJ) (844606) and by the State of Styria (Styrian Funding Agency SFG) (1 .000.038.674). COMET is managed by the Austrian Research Promotion Agency FFG.

References

- [1] K. Masters, *Spray Drying in Practice*(Charlottenlund) 2002.
- [2] J. Dlouhy, W.H. Gauvin, *Heat and Mass Transfer in Spray Drying*, McGill University, 1957.
- [3] A. Mujumdar, *Handbook of Industrial Drying*, Fourth Edition vol. 4, CRC Press, 2015.
- [4] R. Vehring, *Pharmaceutical particle engineering via spray drying*, *Pharm. Res.* 25 (5) (2008) 999–1022.
- [5] P.C. Nordine, R.M. Atkins, *Aerodynamic levitation of laser-heated solids in gas jets*, *Rev. Sci. Instrum.* 53 (9) (1982) 1456–1464.
- [6] G.D. Kinzer, R. Gunn, *The evaporation, temperature and thermal relaxation-time of freely falling waterdrops*, *J. Meteorol.* 8 (2) (1951) 71–83.
- [7] W.E. Ranz, W.R. Marshall, *Evaporation from drops - part I*, *Chem. Eng. Pro* 48 (3) (1952) 141–146.
- [8] D.H. Charlesworth, W.R. Marshall, *Evaporation from drops containing dissolved solids*, *AIChE J.* 6 (1) (1960) 9–23.
- [9] N. Tsapis, et al., *Onset of buckling in drying droplets of colloidal suspensions*, *Phys. Rev. Lett.* 94 (1) (2005) 18302.
- [10] E. James Davis, P. Ravindran, A.K. Ray, *Single aerosol particle studies*, *Adv. Colloid Interf. Sci.* 15 (1) (1981) 1–24.
- [11] E.J. Davis, G. Schweiger, *The Airborne Microparticle*, Springer Berlin Heidelberg, Berlin, Heidelberg, 2002.
- [12] G. Brenn, L.J. Deviprasath, F. Durst, C. Fink, *Evaporation of acoustically levitated multi-component liquid droplets*, *Int. J. Heat Mass Transf.* 50 (25–26) (2007) 5073–5086.
- [13] H. Schiffer, G. Lee, *Single-droplet evaporation kinetics and particle formation in an acoustic levitator. Part 2: drying kinetics and particle formation from microdroplets of aqueous mannitol, trehalose, or catalase*, *J. Pharm. Sci.* 96 (9) (2007) 2284–2295.
- [14] O. Kastner, G. Brenn, D. Rensink, C. Tropea, *The acoustic tube levitator - a novel device for determining the drying kinetics of single droplets*, *Chem. Eng. Technol.* 24 (4) (2001) 335–339.
- [15] H.A. Schiffer, *Single Droplet Drying of Proteins and Protein Formulations Via Acoustic Levitation*, Friedrich-Alexander University Erlangen-Nürnberg, 2006.
- [16] F. Priego-Capote, L. de Castro, *Ultrasound-assisted levitation: lab-on-a-drop*, *TrAC Trends Anal. Chem.* 25 (9) (2006) 856–867.
- [17] E.G. Lierke, *Akustische Positionierung - Ein umfassender Überblick über Grundlagen und Anwendungen*, *Acustica* 82 (1996) 220–237.
- [18] A. Anilkumar, C. Lee, T. Wang, *Stability of an acoustically levitated and flattened drop: an experimental study*, *Phys. Fluids A Fluid Dyn.* 5 (11) (1993) 2763–2775.
- [19] S. Santesson, S. Nilsson, *Airborne chemistry: acoustic levitation in chemical analysis*, *Anal. Bioanal. Chem.* 378 (7) (2004) 1704–1709.
- [20] A.L. Yarin, G. Brenn, O. Kastner, D. Rensink, C. Tropea, *Evaporation of acoustically levitated droplets*, *J. Fluid Mech.* 399 (1999) 151–204.
- [21] A.L. Yarin, G. Brenn, O. Kastner, C. Tropea, *Drying of acoustically levitated droplets of liquid-solid suspensions: evaporation and crust formation*, *Phys. Fluids* 14 (7) (2002) 2289–2298.
- [22] A.L. Yarin, G. Brenn, D. Rensink, *Evaporation of acoustically levitated droplets of binary liquid mixtures*, *Int. J. Heat Fluid Flow* 23 (4) (2002) 471–486.
- [23] S. Sacher, G. Krammer, *The influence of shear stress on crystallization in an ultrasound levitator*, *Chem. Eng. Technol.* 30 (10) (2007) 1412–1417.
- [24] G. Brenn, *Concentration fields in evaporating droplets*, *Int. J. Heat Mass Transf.* 48 (2) (2005) 395–402.
- [25] N. Kawahara, A.L. Yarin, G. Brenn, O. Kastner, F. Durst, *Effect of acoustic streaming on the mass transfer from a sublimating sphere*, *Phys. Fluids* 12 (4) (2000) 912.

- [26] S. Mascia, et al., End-to-end continuous manufacturing of pharmaceuticals: Integrated synthesis, purification, and final dosage formation, *Angew. Chemie - Int. Ed.* 52 (47) (2013) 12359–12363.
- [27] S. Lawton, G. Steele, P. Shering, L. Zhao, I. Laird, X.W. Ni, Continuous crystallization of pharmaceuticals using a continuous oscillatory baffled crystallizer, *Org. Process. Res. Dev.* 13 (6) (2009) 1357–1363.
- [28] J. Gursch, et al., Continuous processing of active pharmaceutical ingredients suspensions via dynamic cross-flow filtration, *J. Pharm. Sci.* 104 (10) (2015) 3481–3489.
- [29] J. Gursch, et al., Dynamic cross-flow filtration: enhanced continuous small-scale solid-liquid separation, *Drug Dev. Ind. Pharm.* 42 (6) (2016) 977–984.
- [30] J. Gursch, et al., Continuous drying of small particles for pharmaceutical applications - an evaluation of selected lab-scale systems, *Org. Process. Res. Dev.* 19 (12) (2015) 2055–2066.
- [31] M. Kreimer, I. Aigner, G. Koscher, D. Lepek, J.G. Khinast, Continuous drying of powders and slurries in an extruder without changing product particle size distribution, *AIChE Annual Meeting*, 2016.
- [32] J.W. Carson, B.H. Pittenger, Bulk properties of powders, *ASM Handb. Vol. 7, Powder Met. Technol. Appl.*, vol. 7, 1998, pp. 148–159.
- [33] R.C. Rowe, R.J. Roberts, The mechanical properties of powders, *Adv. Pharm. Sci.* 7 (1995) 1–62.
- [34] C. Oliver, M. Pharr, An improved technique for determining hardness and elastic modulus using load and displacement sensing indentation experiments, *J. Mater. Res.* 7 (11) (1992) 1564–1583.
- [35] L.J. Taylor, et al., Predictive milling of pharmaceutical materials using nanoindentation of single crystals, *Org. Process. Res. Dev.* 8 (4) (2004) 674–679.
- [36] L. Taylor, D. Papadopoulos, P. Dunn, A. Bentham, J. Mitchell, M. Snowden, Mechanical characterisation of powders using nanoindentation, *Powder Technol.* 143–144 (2004) 179–185.
- [37] M. Perkins, et al., Elastic modulus measurements from individual lactose particles using atomic force microscopy, *Int. J. Pharm.* 332 (1–2) (2007) 168–175.
- [38] X. Liao, T.S. Wiedmann, Measurement of process-dependent material properties of pharmaceutical solids by nanoindentation, *J. Pharm. Sci.* 94 (1) (2005) 79–92.
- [39] K.J. Ramos, D.F. Bahr, Mechanical behavior assessment of sucrose using nanoindentation, *J. Mater. Res.* 22 (7) (2007) 2037–2045.
- [40] X. Liao, T.S. Wiedmann, Characterization of pharmaceutical solids by scanning probe microscopy, *J. Pharm. Sci.* 93 (9) (2004) 2250–2258.
- [41] V.M. Masterson, X. Cao, Evaluating particle hardness of pharmaceutical solids using AFM nanoindentation, *Int. J. Pharm.* 362 (1–2) (2008) 163–171.
- [42] I.C. van den Born, A. Santen, H.D. Hoekstra, J.T.M. De Hosson, Mechanical strength of highly porous ceramics, *Phys. Rev. B Condens. Matter* 43 (4) (1991) 3794–3796.
- [43] C. Couroyer, Methodology for investigating the mechanical strength of reforming catalyst beads, *Oil Gas Sci. Technol. Rev. Institut Fr. Dupetrole* 55 (1) (2000) 67.
- [44] N. Rahmanian, M. Ghadiri, Y. Ding, Effect of scale of operation on granule strength in high shear granulators, *Chem. Eng. Sci.* 63 (4) (2008) 915–923.
- [45] N. Rahmanian, M. Ghadiri, X. Jia, F. Stepanek, Characterisation of granule structure and strength made in a high shear granulator, *Powder Technol.* 192 (2) (2009) 184–194.
- [46] N. Rahmanian, A. Naji, M. Ghadiri, Effects of process parameters on granules properties produced in a high shear granulator, *Chem. Eng. Res. Des.* 89 (5) (2011) 512–518.
- [47] N. Rahmanian, M. Ghadiri, Strength and structure of granules produced in continuous granulators, *Powder Technol.* 233 (2013) 227–233.
- [48] J.J. Machado, J.A. Coutinho, E.A. Macedo, Solid-liquid equilibrium of α -lactose in ethanol/water, *Fluid Phase Equilib.* 173 (1) (2000) 121–134.
- [49] F. Montañés, A. Olano, E. Ibáñez, T. Fornari, Modeling solubilities of sugars in alcohols based on original experimental data, *AIChE J.* 53 (9) (2007) 2411–2418.
- [50] G. Brenn, *Analytical Solutions for Transport Processes*, Springer Berlin Heidelberg, Berlin, Heidelberg, 2017.
- [51] H.J. Ryu, F. Saito, Single particle crushing of nonmetallic inorganic brittle materials, *Solid State Ionics* 47 (1–2) (1991) 35–50.
- [52] C. Gauge, T.S. Anvils, Standard Test Method for Single Pellet Crush Strength of Formed Catalysts and Catalyst Carriers ASTM D4179-11 2011.
- [53] Y. Tian, R.G. Holt, R.E. Apfel, Deformation and location of an acoustically levitated liquid drop, *J. Acoust. Soc. Am.* 93 (6) (1993) 3096–3104.
- [54] S. Zhao, J. Wallaschek, A standing wave acoustic levitation system for large planar objects, *Arch. Appl. Mech.* 81 (2) (2011) 123–139.
- [55] W.M. Haynes, *CRC Handbook of Chemistry and Physics*, 97th Edition CRC Press, 2016.
- [56] S.J. Ashcroft, A.D. Clayton, R.B. Shearn, Isothermal vapor-liquid equilibria for the systems toluene-n-heptane, toluene-propan-2-ol, toluene-sulfolane, and propan-2-ol-sulfolane, *J. Chem. Eng. Data* 24 (3) (1979) 195–199.
- [57] K. Sefiane, L. Tadrist, M. Douglas, Experimental study of evaporating water-ethanol mixture sessile drop: influence of concentration, *Int. J. Heat Mass Transf.* 46 (23) (2003) 4527–4534.
- [58] K. Hasegawa, Y. Abe, A. Goda, Microlayered flow structure around an acoustically levitated droplet under a phase-change process, *npj Microgravity* 2 (1) (2016) 16004.
- [59] R. Vehring, W.R. Foss, D. Lechuga-Ballesteros, Particle formation in spray drying, *J. Aerosol Sci.* 38 (2007) 728–746.
- [60] S.J. Lukasiewicz, Spray-drying ceramic powders, *J. Am. Ceram. Soc.* 72 (4) (1989) 617–624.
- [61] G. Bertrand, P. Roy, C. Filiatre, C. Coddet, Spray-dried ceramic powders: a quantitative correlation between slurry characteristics and shapes of the granules, *Chem. Eng. Sci.* 60 (1) (2005) 95–102.
- [62] E. Wulsten, F. Kiekens, F. van Dycke, J. Voorspoels, G. Lee, Levitated single-droplet drying: case study with itraconazole dried in binary organic solvent mixtures, *Int. J. Pharm.* 378 (1–2) (2009) 116–121.